Quantifying the effects of hydration on corneal stiffness with noncontact optical coherence elastography

Manmohan Singh, BSc, **Zhaolong Han, PhD**, **Jiasong Li, PhD**, **Srilatha Vantipalli, PhD**, **Salavat R. Aglyamov, MSc, PhD**, **Michael D. Twa, OD, PhD**, and **Kirill V. Larin, MSc, PhD**

Biomedical Engineering (Singh, Li, Larin) and the College of Optometry (Vantipalli), Mechanical Engineering (Aglyamov), University of Houston, and Molecular Physiology and Biophysics (Larin), Baylor College of Medicine, Houston, Texas, and the School of Optometry (Twa) and Biomedical Engineering (Twa), University of Alabama at Birmingham, Birmingham, Alabama, USA; the School of Naval Architecture (Han), Ocean and Civil Engineering, Shanghai Jiao Tong University, Shanghai, China; Interdisciplinary Laboratory of Biophotonics (Larin), Tomsk State University, Tomsk, Russia

Abstract

PURPOSE—To quantify the effects of the hydration state on the Young's modulus of the cornea.

SETTING—Biomedical Optics Laboratory, University of Houston, Houston, Texas, USA.

DESIGN—Experimental study.

METHODS—Noncontact, dynamic optical coherence elastography (OCE) measurements were taken of in situ rabbit corneas in the whole eye–globe configuration (n = 10) and at an artificially controlled intraocular pressure of 15 mm Hg. Baseline OCE measurements were taken by topically hydrating the corneas with saline for 1 hour. The corneas were then dehydrated topically with a 20% dextran solution for another hour, and the OCE measurements were repeated. A finite element method was used to quantify the Young's modulus of the corneas based on the OCE measurements.

RESULTS—The thickness of the corneas shrank considerably after topical addition of the 20% dextran solution (~680 μm to ~370 μm), and the OCE-measured elastic-wave speed correspondingly decreased (~3.2 m/s to ~2.6 m/s). The finite element method results showed an increase in Young's modulus (500 kPa to 800 kPa) resulting from dehydration and subsequent thinning.

Corresponding author: Kirill V. Larin, MSc, PhD, Department of Biomedical Engineering, University of Houston, 3517 Cullen Boulevard, Room 2027, Houston, Texas 77204, USA. klarin@uh.edu.
Drs. Singh and Han contributed equally to this work

CONCLUSION—Young's modulus increased significantly as the corneas dehydrated and thinned, showing that corneal geometry and hydration state are critical factors for accurately quantifying corneal biomechanical properties.

The cornea is a crucial part of vision because it provides physical protection to delicate inner elements of the eye and approximately two thirds of the total refractive power of the eye.[1] The structural integrity of corneal tissue is vital to its function and subsequent visual health by maintaining proper corneal geometry. It is well known that the corneal biomechanical properties and corneal geometry are tightly linked.[2] Diseases such as keratoconus[3] and refractive procedures such as laser in situ keratomileusis[4] and ultraviolet-A with riboflavin corneal crosslinking (CXL)[5] can alter corneal biomechanical properties and geometry, leading to changes in visual acuity. For example, keratoconus causes degeneration of the cornea, leading to a highly irregular corneal geometry that results in distorted vision.[6,7] In general, keratoconus is diagnosed by techniques that rely on detecting these morphologic abnormalities and resulting visual aberrations.[7–9] However, techniques that can measure corneal biomechanical properties would enable earlier detection of disease onset by identifying underlying changes in corneal biomechanical properties before noticeable morphologic aberrations develop. Moreover, CXL is intended to stiffen the cornea; thus, evaluating corneal biomechanical properties could provide for planning and evaluating custom CXL therapies.[10,11] However, quantifying corneal biomechanical properties is not a simple process. Numerous confounding factors must be considered; these include corneal geometry, intraocular pressure (IOP), mechanical anisotropy, and nonlinearity.[12–21] Isolating and understanding the effects of these parameters is crucial for developing methods to accurately quantify corneal biomechanical properties.

Although the relationship between corneal hydration and thickness has been well studied, are fewer studies have assessed the relationship between corneal dehydration and biomechanical properties. Previous studies have used atomic force microscopy (AFM),[22] inflation testing,[23] uniaxial mechanical testing,[24] and compression testing[25] to evaluate changes in corneal biomechanical properties resulting from altered hydration states. However, these modalities are not well suited to in vivo applications because of the destructive nature of mechanical and inflation testing, the long imaging times of AFM,[26] and the complications associated with assessments of compression.[27,28] Another reason to study the effects of dehydration on corneal biomechanical properties is the traditional CXL protocol,[5] in which a 20% dextran solution is used. Previous studies have brought the effects of tissue dehydration as a compounding factor of the CXL stiffening into question[29,30] and have shown seemingly contradictory results of the effects of hydration on corneal stiffness.[22–25] Thus, understanding the effects of dehydration is crucial, not only for understanding inherent corneal biomechanical properties but also the effects of therapies such as CXL.

Measuring the biomechanical parameters of the cornea presents a challenge because of the cornea's nonlinear viscoelastic behavior[31] and noninvasive in vivo measurements are required. Traditional uniaxial testing of the cornea is impossible to perform in vivo because of its destructive nature and it is difficult to replicate in vivo conditions during such measurements.[31] Similarly, other mechanical testing techniques, such as inflation testing,[23] are not viable in clinical applications. Clinically available instruments, such as the Ocular

Response Analyzer (Reichert Technologies) and Corvis ST (Oculus Surgical, Inc.), use a large-force air puff to displace the cornea and quantify various parameters, such as inward deflection speed and corneal hysteresis. Although these parameters can be informative for disease detection, there is disagreement about their ability to detect changes in corneal biomechanical properties resulting from pathology, treatment, or both.[4,32–36] Brillouin microscopy can also assess the biomechanical properties of tissues noninvasively by measuring the Brillouin shift.[37,38] However, the link between material parameters and the Brillouin shift remains unclear.

Elastography was formalized in the early 1990s to quantify tissue mechanical properties by imaging displacements in tissues and then quantifying tissue biomechanical properties by linking the imaged displacements to mechanical models. Traditional elastographic techniques, such as ultrasound elastography[39] and magnetic resonance elastography,[40] have limited applications for the cornea because of their relatively large displacement amplitudes, poor spatial resolution, cost, and/or need for contact-based excitation. Optical coherence tomography (OCT)–based elastography,[41] which is termed optical coherence elastography (OCE),[42,43] overcomes these limitations with micrometer-scale spatial resolution, nanometer-scale displacement sensitivity,[44] and noncontact excitation. Thus, OCE has been used to characterize the biomechanical properties of bioengineered tissue,[45] prostate cancer samples,[46] fibrotic mouse skin,[47] nephritic mouse kidneys,[48] and breast cancer biopsy samples,[49] among others. In general, the imaging depth of OCT is limited to a few millimeters in tissue; however, because the cornea is less scattering than most tissues and is usually thinner than 1.0 mm, OCT can image the entire thickness of the cornea. Moreover, the high spatial resolution and subnanometer displacement sensitivity make OCE well suited for characterizing corneal biomechanical properties.[43] Contact-based ocular OCE techniques have shown the heterogeneous properties of corneal tissue[50] under various conditions.[51,52] However, noncontact techniques are most favorable for corneal OCE because of their ease of use, lower risk for damaging tissue, and patient comfort.

In our previous studies,[21,53] we used the finite element method combined with OCE measurements of elastic-wave propagation to quantify the Young's modulus of corneal tissue. The finite element method was chosen for its ability to easily adjust geometric parameters critical for accurately quantifying corneal biomechanical properties, such as thickness and curvature,[21] and to integrate appropriate boundary conditions. We have also shown that the quantification of Young's modulus of the cornea is strongly affected by the presence of the fluid–structure interface at the posterior corneal surface[53,54]; therefore, the finite element method combined with OCE measurements shows potential for quantitatively assessing the effects of corneal hydration state on its biomechanical properties accurately.

In this study, we use a focused micro air pulse to induce elastic waves in fresh rabbit corneas in the whole eye–globe configuration. The elastic-wave propagation was detected by OCE, and the changes in corneal thickness and biomechanical properties, as quantified by OCE and the finite element method, during dehydration of the corneal tissue were analyzed.

MATERIALS AND METHODS

Ten fresh mature (>6 months) whole rabbit eye globes (Pel-Freez Biologicals) were shipped overnight on ice. Excess tissues, such as muscles, were removed from the globes, and the corneal epithelium was removed with a blunt surgical instrument. Because IOP can have a strong effect on the measured corneal biomechanical properties,[54,55] it was set with a closed-loop IOP control system to a physiologically relevant 15 mm Hg during all experiments.[56] The globes were placed in a home-built eye holder and were cannulated with 2 needles. One needle was connected via tubing to a pressure transducer, and the other needle was connected via tubing to a micro infusion pump to form the closed-loop IOP control system.

The short duration (<1 millisecond), low pressure (<10 Pa) focused micro air pulse was directed at the apex of the cornea and induced a low amplitude displacement (<10 μm), which then propagated as an elastic wave in the corneal tissue.[57] To ensure that the effects of corneal mechanical anisotropy were excluded,[58,59] all OCE measurements were taken along the nasal–temporal meridian. A 0.9% phosphate-buffered saline (PBS) solution was dropped on the corneas every 5 minutes, and the OCE measurements were taken every 20 minutes to establish a baseline. After the 60-minute measurement, 20% dextran in 0.9% PBS solution was dropped on the corneas every 5 minutes to dehydrate the corneas. The OCE measurements were then taken every 20 minutes for another 1 hour.

The elastic-wave propagation was detected with a phase-stabilized swept-source OCE system, which has been described in detail.[60] Briefly, the system has a central wavelength of approximately 1310 nm, a scan range of approximately 150 nm, a scan rate of 30 kHz, and a phase stability in the cornea of approximately 20 nm. Figure 1 shows a schematic of the system. The M-B-mode imaging was performed by synchronizing the air pulse with the OCT frame trigger, and 251 M-mode images were taken over an approximate 7.0 mm scan.[61] Before any calculations, the phase data were corrected for the refractive index mismatch between the corneal tissue and air[62] with the refractive index of the corneal tissue as 1.376.[63] The elastic-wave group velocity was quantified by cross-correlation analysis of the elastic-wave temporal displacement profiles. The elastic-wave propagation delays, which were determined by cross-correlation, were then linearly fitted to the wave-propagation distances, and the slope of the linear fit was used to calculate the velocity.[64] This procedure was repeated for each imaged in-depth layer, taking the curvature of the cornea into account as an accurate distance for the elastic-wave propagation path. The velocity was then averaged along the entire depth of the cornea for a given measurement. The central corneal thickness (CCT) was measured after the OCT structural image was rescaled to physical dimensions, again assuming a corneal refractive index of 1.376.[63]

Young's modulus was estimated with the finite element method in the Ansys environment software (version 14.0, Ansys, Inc.).[21,53] Based on the OCT structural image obtained during the OCE measurements, the anterior and posterior surfaces of the rabbit cornea were well fitted by a circle. Hence, the finite element model was simplified as a spherical shell, with a curvature from an average of all samples. The mean fitted radius of the anterior surface was $r_{ant} = 7.80 \pm 0.05$ mm, which indicated a negligible change in the corneal

curvature during the experiments. In contrast, the CCT changed significantly, as expected, with a mean CCT of all samples at all timepoints of 571 ± 132 μm, where the error is the standard deviation (SD). The averaged CCTs from all samples for a given timepoint were used in the finite element models. During the simulation, the corneal tissue was assumed as linearly elastic and the Poisson ratio, mass density, aqueous humor density, and speed of sound in fluid were set at 0.49, 1062 kg/m[3,65] 1000 kg/m^{3}, and 1500 m/s, respectively. Fixed boundary conditions were considered at the corneoscleral limbus, and the OCE-measured displacement profile at the corneal apex was applied to the finite element model as an excitation, also at the apex. A fluid–structure interface was prescribed at the posterior surface to integrate the effect of the aqueous humor on the elastic wave in the cornea.[53] In the finite element model, a SOLID186-type element was used to mesh the cornea, and a FLUID220-type element was applied to the aqueous humor. The mesh sizes were 300 μm. The Young's modulus of the finite element model was incrementally changed until the error between the finite element method–calculated velocity and the average OCE-measured velocity for that given timepoint was less than 5%.

RESULTS

Figure 2 shows OCT structural images at the indicated times in a typical sample. There was a slight swelling resulting from the hydration by PBS in this sample; the cornea swelled from 672 μm at the 0-minute measurement to 713 μm at 60 minutes. After the topical addition of the 20% dextran solution, the CCT rapidly shrank from 713 μm at 60 minutes to 387 μm when the measurements were completed at 120 minutes. Figure 3 shows sample frames of the air pulse–induced elastic-wave propagating, as in the sample shown in Figure 2, at the initial 0-minute measurement and at the 100-minute measurement. Video 1 (available at: http://jcrsjournal.org) shows the propagation of the elastic wave at 1000 times slower than real time, with the 0-minute OCE measurement (*top*) and the 100-minute measurement (*bottom*). The times after excitation are shown at the top of each image in Figure 3 and Video 1 (available at: http://jcrsjournal.org). The red region at the apex of the 100-minute measurement is the result of phase-unwrapping errors and was excluded in calculations. The pale blue regions at the periphery of the cornea in Figure 3, *c*, show that the wave had mostly propagated out of the imaged region 2 milliseconds after excitation at the 0-minute measurement. In contrast, the wave is still clearly visible 2 milliseconds after excitation in the 100-minute measurement (Figure 3, *f*), showing that the wave was faster when the cornea was swollen than to when the cornea was dehydrated. Figure 4, *a*, plots the intersample mean CCT and elastic-wave velocity as a function time for all 10 samples with the error bars representing the inter-sample SD. The mean CCT slightly increased from 671 $\pm$ 54 μm at the initial 0-minute measurement to 676 ± 49 μm at the 60-minute measurement. After the addition of the 20% dextran solution, the thickness rapidly shrank to 367 ± 29 μm at the final measurement at 120 minutes. The average elastic-wave velocity decreased from 3.2 ± 0.2 m/s at the first OCE measurement to 2.6 ± 0.2 m/s at the final OCE measurement at 120 minutes.

The finite element method was used to quantify the Young's modulus of the cornea because it can accurately replicate the geometry and boundary conditions of the cornea. Quantifications were made on the averaged data shown in Figure 4, *a*. The mean error

between the OCE-measured and finite element method–computed group velocity was 3.1% ± 5.7%, showing good agreement between the OCE measurements and finite element method results. Figure 4, *b*, plots the changes in CCT as well as the finite element method–assessed Young's modulus as a function of time. From 0 to 60 minutes, when the PBS was dropped on the corneas, the CCT slightly increased and Young's modulus decreased slightly from 500 kPa to 465 kPa. However, the addition of the 20% dextran solution caused the cornea to thin significantly, from approximately 680 μm at 60 minutes to approximately 370 μm at 120 minutes, which caused a corresponding increase in Young's modulus from 465 kPa to 800 kPa.

DISCUSSION

In this study, we used a focused micro air pulse to induce low-amplitude elastic waves in the cornea; the waves were detected by a phase-stabilized OCE system. The OCE-measured elastic-wave velocity and OCT-measured corneal geometry were then used in finite element models to quantify the Young's modulus of the cornea while it was dehydrated with a 20% dextran solution. The Young's modulus of the cornea increased significantly as the corneas dehydrated and thinned. The main advantages of our work are that we (1) induced very small displacements (micrometer scale) to avoid global eye globe deformation during the OCE measurements,[31] (2) used a constant IOP to eliminate variations in OCE-measured corneal biomechanical properties resulting from IOP changes,[31,54,55, 66] (3) performed all measurements in the whole-globe configuration to avoid ambiguities resulting from different corneal tissue preparation methods,[22] and (4) quantified the Young's modulus of the cornea with a widely used engineering technique.[36–38,54]

The corneas were topically hydrated with a 0.9% PBS solution, which is hypotonic to the corneal stroma and causes slight swelling. Normally, rabbit corneas are approximately 400 μm thick[67]; however, they were approximately 670 μm after storage and hydration with PBS and deepithelialization. Previous studies[22,23] found positive correlations between corneal thickness and stiffness. Kling and Marcos[23] used inflation testing and found that the slope of the change in corneal thickness versus IOP was flatter in corneas stored in a 20% dextran solution than in untreated corneas, indicating a decrease in stiffness after storage in 20% dextran and subsequent thinning. However, inflation testing requires large changes in IOP that induce nonlinear biomechanical responses and no material parameters were quantified. Dias and Ziebarth[22] used AFM to perform indentation testing and found that a 15% dextran solution thinned the corneas and caused the smallest increase in corneal stiffness compared with saline solutions. In contrast, Cherfan et al.[68] used mechanical extensiometry and found that riboflavin 0.1% in 20% dextran solution increased the Young's modulus of the cornea by more than 2 times. Hatami-Marbini and Rahimi[24,69] showed that the tangential elastic modulus of corneal strips increased as thickness decreased (ie, the corneas were dehydrated) using mechanical extensiometry and that the in-plane and out-of-plane Young's moduli increased as corneal tissue hydration decreased with mechanical compression testing.[25] The differences in the spatial and temporal scales of the measurement can bring about seemingly contradictory results. Cancer is the most notable example. Macrostructural elastography has shown that tumors are stiffer than surrounding tissue[70,71]; however, microscale and nanoscale measurements have shown that malignant cells are softer than healthy cells.[72,73]

Thus, the assessments of Dias and Ziebarth[22] using AFM are not actually contradictory to the work by others showing that the bulk corneal stiffness increased when the cornea was dehydrated. Therefore, future study will require multiscale evaluation of corneal biomechanical properties to understand the changes at the tissue, cellular, and subcellular scales as a function of hydration.

Our previous work with OCE and the finite element method showed that as the thickness of agar phantoms increased, the OCE-measured and finite element method–simulated wave speeds increased when Young's modulus was held constant.[21] The results in this study show the same trend; however, Young's modulus followed the opposite trend, indicating that wave speed alone is not truly indicative of the cornea's material properties. If the Young's modulus of the cornea were to remain constant, the changes in wave speed would perhaps be more dramatic. Additional simulations were performed by changing the thickness of corneal finite element models within the range observed in this study (~400 μm to ~800 μm) at a fixed Young's modulus of 500 kPa (data not shown). These results showed a much more pronounced change in wave speed (~2.5 m/s at ~400 μm to ~4.5 m/s at ~800 μm) than the OCE-measured wave speed in the in situ porcine corneas. Thus, there was a change in the Young's modulus of the cornea that compensated for the significant change in CCT. At the same IOP, a decrease in CCT could increase the stress on the corneal tissue. Because the cornea has a characteristic J- shaped stress–strain curve,[31] the additional stress could cause an increase in Young's modulus. Although the radius of curvature can also affect the measured wave speed,[21] an analysis of variance test showed no significant variation in the radius of curvature as a function of CCT ($P = .234$); thus, no further analysis was performed.

An additional outcome of our results is the error that can be introduced when quantifying corneal biomechanical properties without accounting for the thickness. We performed finite element method simulations in which Young's modulus and the thickness were altered so that the group velocity was equal (data not shown). The finite element method simulations matched results from our previously developed modified Rayleigh-Lamb wave model for the cornea[54,74] with the same parameters. Here, a small change in thickness of 80 μm resulted in a large difference in Young's modulus of 210 kPa when the velocity was equal (at ~2.8 m/s). Therefore, even though a similar velocity is measured in the cornea, the Young's modulus can be quite different for a different thickness.

The absolute values of Young's modulus quantified in this study is higher than in our own previous work with rabbit corneas.[53,75] In fact, the reported values of Young's modulus of the cornea vary by several orders of magnitude,[76] from a few kilopascals as assessed by AFM[77] to tens of megapascals as measured by tensile testing.[78] Multiple factors can account for this wide range of values, including the nonlinear stress–strain curve of the cornea,[31] the testing conditions that can artificially raise the "equivalent IOP"[31] and the temporal and spatial scale of the measurement.

In a live animal, the endothelial pumps, which help control corneal hydration and thickness, are still functioning. In ex vivo conditions, the pumps cease to function and various solutions have been tested to maintain corneal thickness.[22,79,80] In our future work, we will evaluate such solutions and their ability to control corneal thickness and their subsequent effects on

corneal biomechanical properties as well as in vivo testing of how the corneal hydration state alters biomechanical properties. Moreover, the corneal hydration state and mass density are tightly linked.[81] In this study, we kept the density constant, assuming its influence on the results would be minimal because of the relatively small influence of density on the Young's modulus in many wave models.[54,82,83] We will integrate the changes in density to our future calculations.

A major limitation of this study is the quantification of corneal viscoelastic properties. At present, our combined technique of air-pulse OCE and the finite element method can only provide Young's modulus but not the viscosity. We have shown that the elastic-wave group velocity depends on the thickness of the material, even when all other parameters, including the Young's modulus, are equal.[21] Group velocity has often been used to quantify the Young's modulus of the cornea with simple models, primarily the shear-wave and surface-wave models. However, those models assume the sample is an infinitely thick plate,[83] which the cornea is not. We have developed a modified Rayleigh-Lamb wave model that uses the spectral dispersion of the elastic wave, considers the thickness of the sample, and integrates the fluid–structure interface at the corneal posterior surface to quantify the Young's modulus and shear viscosity of the cornea, but this model assumes the cornea is a flat thin plate.[54,74] Hence, the finite element method was used because it can accurately replicate the corneal geometry, including curvature, which is an advantage of the finite element method over most analytical wave models. However, the OCE and finite-element method technique we present is based on group velocity only and cannot be used to obtain the viscosity of the cornea tissue because there would be 2 unknowns (Young's modulus and viscosity) with only 1 known parameter (elastic-wave group velocity). The next step of our work is to integrate the OCE-measured elastic-wave spectral dispersion[84–86] into the finite element method simulations to obtain the viscoelasticity; however, this will increase the finite element method simulation time significantly.

Another limitation is the OCE acquisition time, which is tens of seconds. The extended acquisition time and need for multiple excitations would not be satisfactory for patient comfort. In additional, M-mode imaging means that corneal laser safety limits were exceeded. We developed an ultrafast technique capable of detecting the elastic-wave propagation within milliseconds, with only 1 excitation, and within corneal laser safety exposure limits.[66,87] However, the transverse spatial resolution is still limited. Nevertheless, this technique might be sufficient when combined with the finite element method or an accurate analytical wave model to quantify the biomechanical properties of the cornea within milliseconds in a completely noninvasive and safe manner.

In conclusion, this study found that the thickness of in situ rabbit corneas decreased along with the air pulse–induced elastic-wave velocity after the corneas were dehydrated with a 20% dextran solution. Quantification of Young's modulus by the finite element method showed that the cornea stiffens as it dehydrates and reduces in thickness. The results indicate that the hydration state of the cornea plays a noticeable role in corneal biomechanical properties, which is particularly important for therapies such as CXL in which dextran solution is used.

Supplementary Material

Refer to Web version on PubMed Central for supplementary material.

Acknowledgments

References

1. Ruberti JW, Sinha Roy A, Roberts CJ. Corneal biomechanics and biomaterials. Annu Rev Biomed Eng. 2011; 13:269–295. [PubMed: 21568714]

2. Mas Tur V, MacGregor C, Jayaswal R, O'Brart D, Maycock N. A review of keratoconus: diagnosis, pathophysiology and genetics. Surv Ophthalmol. 2017; 62:770–783. [Accessed May 21, 2018] Available at: https://www.surveyophthalmol.com/article/S0039-6257(17)30046-2/pdf. [PubMed: 28688894]

3. Wang L-K, Tian L, Zheng Y-P. Determining in vivo elasticity and viscosity with dynamic Scheimpflug imaging analysis in keratoconic and healthy eyes. J Biophotonics. 2016; 9:454–463. [PubMed: 26755237]

4. Ortiz D, Piñero D, Shabayek MH, Arnalich-Montiel F, Alió JL. Corneal biomechanical properties in normal, post-laser in situ keratomileusis, and keratoconic eyes. J Cataract Refract Surg. 2007; 33:1371–1375. [PubMed: 17662426]

5. Wollensak G, Spoerl E, Seiler T. Riboflavin/ultraviolet-A–induced collagen crosslinking for the treatment of keratoconus. Am J Ophthalmol. 2003; 135:620–627. [Accessed May 21, 2018] Available at: http://s499648585.mialojamiento.es/biblioteca/CROSS-LINKING/Wollensak%20et%20al%20Keratoconus%202003.pdf. [PubMed: 12719068]

6. Kennedy RH, Bourne WM, Dyer JA. A 48-year clinical and epidemiologic study of keratoconus. Am J Ophthalmol. 1986; 101:267–273. [PubMed: 3513592]

7. Alió JL, editorKeratoconus;p Recent Advances in Diagnosis and Treatment. Cham, Switzerland: Springer International Publishing; 2017.

8. Mahmoud AM, Nuñez MX, Blanco C, Koch DD, Wang L, Weikert MP, Frueh BE, Tappeiner C, Twa MD, Roberts CJ. Expanding the cone location and magnitude index to include corneal thickness and posterior surface information for the detection of keratoconus. Am J Ophthalmol. 2013; 156:1102–1111. [PubMed: 24075426]

9. Twa MD, Parthasarathy S, Roberts C, Mahmood AM, Raasch TW, Bullimore MA. Automated decision tree classification of corneal shape. Optom Vis Sci. 2005; 82:1038–1046. [Accessed May 21, 2018] Available at: http://www.ncbi.nlm.nih.gov/pmc/articles/PMC3073139/pdf/nihms275710.pdf. [PubMed: 16357645]

10. Singh M, Li J, Vantipalli S, Han Z, Larin KV, Twa MD. Optical coherence elastography for evaluating customized riboflavin/UV-A corneal collagen crosslinking. J Biomed Opt. 2017; 22:91504. [PubMed: 28055060]

11. Seiler TG, Fischinger I, Koller T, Zapp D, Frueh BE, Seiler T. Customized corneal cross-linking: one-year results. Am J Ophthalmol. 2016; 166:14–21. [PubMed: 26944278]

12. Huseynova T, Waring GO IV, Roberts C, Krueger RR, Tomita M. Corneal biomechanics as a function of intraocular pressure and pachymetry by dynamic infrared signal and Scheimpflug imaging analysis in normal eyes. Am J Ophthalmol. 2014; 157:885–893. [PubMed: 24388837]

13. Bao F, Deng M, Wang Q, Huang J, Yang J, Whitford C, Geraghty B, Yu A, Elsheikh A. Evaluation of the relationship of corneal biomechanical metrics with physical intraocular pressure and central corneal thickness in ex vivo rabbit eye globes. Exp Eye Res. 2015; 137:11–17. [PubMed: 26026878]

14. Vinciguerra R, Elsheikh A, Roberts CJ, Ambrósio R Jr, Kang DSY, Lopes BT, Morenghi E, Azzolini C, Vinciguerra P. Influence of pachymetry and intraocular pressure on dynamic corneal response parameters in healthy patients. J Refract Surg. 2016; 32:550–561. [Accessed May 21, 2018] Available at: https://www.healio.com/ophthalmology/journals/jrs/

2016-8-32-8/%7B78250870-3d63-4f32-846b-d4fb65f8070f%7D/influence-of-pachymetry-and-intraocular-pressure-on-dynamic-corneal-response-parameters-in-healthy-patients.pdf. [PubMed: 27505316]

15. Karimi A, Razaghi R, Navidbakhsh M, Sera T, Kudo S. Computing the influences of different intraocular pressures on the human eye components using computational fluid-structure interaction model. Technol Health Care. 2017; 25:285–297. [PubMed: 27911345]

16. Zhou B, Sit AJ, Zhang X. Noninvasive measurement of wave speed of porcine cornea in ex vivo porcine eyes for various intraocular pressures. Ultrasonics. 2017; 81:86–92. [PubMed: 28618301]

17. Orssengo GJ, Pye DC. Determination of the true intraocular pressure and modulus of elasticity of the human cornea in vivo. Bull Math Biol. 1999; 61:551–572. [PubMed: 17883231]

18. Kling S, Bekesi N, Dorronsoro C, Pascual D, Marcos S. Corneal viscoelastic properties from finite-element analysis of in vivo air-puff deformation. PLoS One. 2014; 9(8):e104904. [Accessed May 21, 2018] Available at: http://www.plosone.org/article/fetchObject.action?uri=info%3Adoi%2F10.1371%2Fjournal.pone.0104904&representation=PDF. [PubMed: 25121496]

19. Bekesi N, Dorronsoro C, de la Hoz A, Marcos S. Material properties from air puff corneal deformation by numerical simulations on model corneas. PLoS One. 2016; 11(10):e0165669. [Accessed May 21, 2018] Available at: https://www.ncbi.nlm.nih.gov/pmc/articles/PMC5085055/pdf/pone.0165669.pdf. [PubMed: 27792759]

20. Kling S, Marcos S. Contributing factors to corneal deformation in air puff measurements. Invest Ophthalmol Vis Sci. 2013; 54:5078–5085. [Accessed May 21, 2018] Available at: http://iovs.arvojournals.org/article.aspx?articleid=2129071. [PubMed: 23821200]

21. Han Z, Li J, Singh M, Aglyamov SR, Wu C, Liu C-h, Larin KV. Analysis of the effects of curvature and thickness on elastic wave velocity in cornea-like structures by finite element modeling and optical coherence elastography. Appl Phys Lett. 2015; 106:233702. [Accessed May 21, 2018] Available at: https://www.ncbi.nlm.nih.gov/pmc/articles/PMC4464060/pdf/APPLAB-000106-233702_1.pdf. [PubMed: 26130825]

22. Dias J, Ziebarth NM. Impact of hydration media on ex vivo corneal elasticity measurements. Eye Contact Lens. 2015; 41:281–286. [Accessed May 21, 2018] Available at https://www.ncbi.nlm.nih.gov/pmc/articles/PMC4506896/pdf/nihms638871.pdf. [PubMed: 25603443]

23. Kling S, Marcos S. Effect of hydration state and storage media on corneal biomechanical response from in vitro inflation tests. J Refract Surg. 2013; 29:490–497. [PubMed: 23820232]

24. Hatami-Marbini H, Rahimi A. The relation between hydration and mechanical behavior of bovine cornea in tension. J Mech Behav Biomed Mater. 2014; 36:90–97. [Accessed May 21, 2018] Available at: https://pdfs.semanticscholar.org/3f52/70aded71c51845b6f003ebc5b40c5415d906.pdf. [PubMed: 24814185]

25. Hatami-Marbini H, Etebu E. Hydration dependent biomechanical properties of the corneal stroma. Exp Eye Res. 2013; 116:47–54. [PubMed: 23891861]

26. Lydataki S, Tsilimbaris MK, Lesniewska ES, Bron A, Pallikaris IG. Corneal tissue observed by atomic force microscopy. In: Braga PC, Ricci D, editorsAtomic Force Microscopy; Biomedical Methods and Applications. Totowa, NJ: Humana Press; 2004. 69–83.

27. Whitacre MM, Stein R. Sources of error with the use of Goldmann-type tonometers. Surv Ophthalmol. 1993; 38:1–30. [PubMed: 8235993]

28. Wijesinghe P, Sampson DD, Kennedy BF. Computational optical palpation: a finite-element approach to micro-scale tactile imaging using a compliant sensor. J R Soc Interface. 2017; 14:20160878. [Accessed May 21, 2018] Available at: https://www.ncbi.nlm.nih.gov/pmc/articles/PMC5378127/pdf/rsif20160878.pdf. [PubMed: 28250098]

29. Hayes S, Boote C, Kamma-Lorger CS, Rajan MS, Harris J, Dooley E, Hawksworth N, Hiller J, Terill NJ, Hafezi F, Brahma AK, Quantock AJ, Meek KM. Riboflavin/UVA collagen cross-linking-induced changes in normal and keratoconus corneal stroma. PLoS One. 2011; 6(8):e22405. [Accessed May 21, 2018] Available at: https://www.ncbi.nlm.nih.gov/pmc/articles/PMC3151245/pdf/pone.0022405.pdf. [PubMed: 21850225]

30. Hatami-Marbini H, Rahimi A. Stiffening effects of riboflavin/UVA corneal collagen cross-linking is hydration dependent. J Biomech. 2015; 48:1052–1057. [PubMed: 25704532]

31. Hoeltzel DA, Altman P, Buzard K, Choe K-i. Strip extensiometry for comparison of the mechanical response of bovine, rabbit, and human corneas. J Biomech Eng. 1992; 114:202–215. [Accessed May 21, 2018] Available at: http://www.buzard.info/StripExtensiometry.pdf. [PubMed: 1602763]

32. Bak-Nielsen S, Pedersen IB, Ivarsen A, Hjortdal J. Dynamic Scheimpflug-based assessment of keratoconus and the effects of corneal cross-linking. J Refract Surg. 2014; 30:408–414. [PubMed: 24972407]

33. Shah S, Laiquzzaman M, Bhojwani R, Mantry S, Cunliffe I. Assessment of the biomechanical properties of the cornea with the Ocular Response Analyzer in normal and keratoconic eyes. Invest Ophthalmol Vis Sci. 2007; 48:3026–3031. [Accessed May 21, 2018] Available at: http://iovs.arvojournals.org/article.aspx?articleid=2183864. [PubMed: 17591868]

34. Gkika M, Labiris G, Giarmoukakis A, Koutsogianni A, Kozobolis V. Evaluation of corneal hysteresis and corneal resistance factor after corneal cross-linking for keratoconus. Graefes Arch Clin Exp Ophthalmol. 2012; 250:565–573. [PubMed: 22189856]

35. Greenstein SA, Fry KL, Hersh PS. In vivo biomechanical changes after corneal collagen crosslinking for keratoconus and corneal ectasia: 1-year analysis of a randomized, controlled, clinical trial. Cornea. 2012; 31:21–25. [PubMed: 21993470]

36. Goldich Y, Barkana Y, Morad Y, Hartstein M, Avni I, Zadok D. Can we measure corneal biomechanical changes after collagen cross-linking in eyes with keratoconus?—A pilot study. Cornea. 2009; 28:498–502. [PubMed: 19421050]

37. Vaughan JM, Randall JT. Brillouin scattering, density and elastic properties of the lens and cornea of the eye [letter]. Nature. 1980; 284:489–491. [PubMed: 7360286]

38. Scarcelli G, Pineda R, Yun SH. Brillouin optical microscopy for corneal biomechanics. Invest Ophthalmol Vis Sci. 2012; 53:185–190. [Accessed May 21, 2018] Available at: http://iovs.arvojournals.org/article.aspx?articleid=2126760. [PubMed: 22159012]

39. Ophir J, Céspedes I, Ponnekanti H, Yazdi Y, Li X. Elastography: a quantitative method for imaging the elasticity of biological tissues. Ultrason Imaging. 1991; 134:111–134.

40. Muthupillai R, Lomas DJ, Rossman PJ, Greenleaf JF, Manduca A, Ehman RL. Magnetic resonance elastography by direct visualization of propagating acoustic strain waves. Science. 1995; 269:1854–1857. [PubMed: 7569924]

41. Huang D, Swanson EA, Lin CP, Schuman JS, Stinson WG, Chang W, Hee MR, Flotte T, Gregory K, Puliafito CA, Fujimoto JG. Optical coherence tomography. Science. 1991; 254:1178–1181. [PubMed: 1957169]

42. Schmitt JM. OCT elastography: imaging microscopic deformation and strain of tissue. Opt Express. 1998; 3:199–211. [Accessed May 21, 2018] Available at: http://www.opticsinfobase.org/oe/viewmedia.cfm?uri=oe-3-6-199&seq=0. [PubMed: 19384362]

43. Larin KV, Sampson DD. Optical coherence elastography – OCT at work in tissue biomechanics [invited]. Biomed Opt Express. 2017; 8:1172–1202. [Accessed May 21, 2018] Available at: https://www.ncbi.nlm.nih.gov/pmc/articles/PMC5330567/pdf/1172.pdf. [PubMed: 28271011]

44. Sticker M, Hitzenberger CK, Leitgeb R, Fercher AF. Quantitative differential phase measurement and imaging in transparent and turbid media by optical coherence tomography. Opt Lett. 2001; 26:518–520. [Accessed May 21, 2018] Available at: ftp://www.astro.gsu.edu/pub/users/shure/papers/downld2/article18.pdf. [PubMed: 18040371]

45. Ko H-J, Tan W, Stack R, Boppart SA. Optical coherence elastography of engineered and developing tissue. Tissue Eng. 2006; 12:63–73. [Accessed May 21, 2018] Available at: http://biophotonics.illinois.edu/pubs/biophotonics_current/elastographyofengineeredtissue.pdf. [PubMed: 16499443]

46. Li C, Guan G, Ling Y, Hsu Y-T, Song S, Huang JT-J, Lang S, Wang RK, Huang Z, Nabi G. Detection and characterisation of biopsy tissue using quantitative optical coherence elastography (OCE) in men with suspected prostate cancer. Cancer Lett. 2015; 357:121–128. [Accessed May 21, 2018] Available at: https://s3.amazonaws.com/academia.edu.documents/45593264/Detection_and_characterisation_of_biopsy20160513-22026-152pyrs.pdf?AWSAccessKeyId=AKIAIWOWYYGZ2Y53UL3A&Expires=1526919080&Signature=rAyP%2BSeFqjiNXwQXOD6Ejd1up%2BQ%3D&response-content-disposition=inline%3B%20filename%3DDetection_and_characterisation_of_biopsy.pdf. [PubMed: 25444932]

47. Du Y, Liu C-H, Lei L, Singh M, Li J, Hicks MJ, Larin KV, Mohan C. Rapid, noninvasive quantitation of skin disease in systemic sclerosis using optical coherence elastography. J Biomed Opt. 2016; 21(4):046002. [Accessed May 21, 2018] Available at: https://www.ncbi.nlm.nih.gov/pmc/articles/PMC4837197/pdf/JBO-021-046002.pdf.

48. Liu C-H, Du Y, Singh M, Wu C, Han Z, Li J, Chang A, Mohan C, Larin KV. Classifying murine glomerulonephritis using optical coherence tomography and optical coherence elastography. J Biophotonics. 2016; 9:781–791. [Accessed May 21, 2018] Available at: https://www.ncbi.nlm.nih.gov/pmc/articles/PMC4956579/pdf/nihms769051.pdf. [PubMed: 26791097]

49. Kennedy KM, Chin L, McLaughlin RA, Latham B, Saunders CM, Sampson DD, Kennedy BF. Quantitative micro-elastography: imaging of tissue elasticity using compression optical coherence elastography. Sci Rep. 2015; 5:15538. [Accessed May 21, 2018] Available at: https://www.ncbi.nlm.nih.gov/pmc/articles/PMC4622092/pdf/srep15538.pdf. [PubMed: 26503225]

50. Ford MR, Dupps WJ Jr, Rollins AM, Sinha Roy A, Hu Z. Method for optical coherence elastography of the cornea. J Biomed Opt. 2011; 16:016005. [Accessed May 21, 2018] Available at: http://www.ncbi.nlm.nih.gov/pmc/articles/PMC3041813/pdf/JBOPFO-000016-016005_1.pdf. [PubMed: 21280911]

51. Ford MR, Sinha Roy A, Rollins AM, Dupps WJ Jr. Serial biomechanical comparison of edematous, normal, and collagen crosslinked human donor corneas using optical coherence elastography. J Cataract Refract Surg. 2014; 40:1041–1047. [Accessed May 21, 2018] Available at: https://www.ncbi.nlm.nih.gov/pmc/articles/PMC4035481/pdf/nihms-578797.pdf. [PubMed: 24767794]

52. Torricelli AAM, Ford MR, Singh V, Santhiago MR, Dupps WJ Jr, Wilson SE. BAC-EDTA transepithelial riboflavin-UVA crosslinking has greater biomechanical stiffening effect than standard epithelium-off in rabbit corneas. Exp Eye Res. 2014; 125:114–117. [Accessed May 21, 2018] Available at: https://www.ncbi.nlm.nih.gov/pmc/articles/PMC4128899/pdf/nihms607542.pdf. [PubMed: 24929203]

53. Han Z, Li J, Singh M, Vantipalli S, Aglyamov SR, Wu C, Liu C-h, Raghunathan R, Twa MD, Larin KV. Analysis of the effect of the fluid-structure interface on elastic wave velocity in cornea-like structures by OCE and FEM. Laser Phys Lett. 2016; 13(3):035602.

54. Han Z, Li J, Singh M, Wu C, Liu C-h, Raghunathan R, Aglyamov SR, Vantipalli S, Twa MD, Larin KV. Optical coherence elastography assessment of corneal viscoelasticity with a modified Rayleigh-Lamb wave model. J Mech Behav Biomed Mater. 2017; 66:87–94. [Accessed May 21, 2018] Available at: https://www.ncbi.nlm.nih.gov/pmc/articles/PMC5182155/pdf/nihms829489.pdf. [PubMed: 27838594]

55. Li J, Han Z, Singh M, Twa MD, Larin KV. Differentiating untreated and cross-linked porcine corneas of the same measured stiffness with optical coherence elastography. J Biomed Opt. 2014; 19(11):110502. Available at: https://www.ncbi.nlm.nih.gov/pmc/articles/PMC4409018/pdf/JBO-019-110502.pdf. [PubMed: 25408955]

56. Twa MD, Li J, Vantipalli S, Singh M, Aglyamov S, Emelianov S, Larin KV. Spatial characterization of corneal biomechanical properties with optical coherence elastography after UV cross-linking. Biomed Opt Express. 2014; 5:1419–1427. [Accessed May 21, 2018] Available at: https://www.ncbi.nlm.nih.gov/pmc/articles/PMC4026912/pdf/1419.pdf. [PubMed: 24877005]

57. Wang S, Larin KV, Li J, Vantipalli S, Manapuram RK, Aglyamov S, Emelianov S, Twa MD. A focused air-pulse system for optical-coherence-tomography-based measurements of tissue elasticity. Laser Phys Lett. 2013; 10:075605. [PubMed: 29805349]

58. Elsheikh A, Brown M, Alhasso D, Rama P, Campanelli M, Garway-Heath D. Experimental assessment of corneal anisotropy. J Refract Surg. 2008; 24:178–187. [Accessed May 21, 2018] Available at: https://m1.healio.com/~/media/journals/jrs/2008/02_february/experimental-assessment-of-corneal-anisotropy-26298/experimental-assessment-of-corneal-anisotropy-26298.pdf. [PubMed: 18297943]

59. Singh M, Li J, Han Z, Raghunathan R, Nair A, Wu C, Liu C-H, Aglyamov S, Twa MD, Larin KV. Assessing the effects of riboflavin/UV-A crosslinking on porcine corneal mechanical anisotropy with optical coherence elastography. Biomed Opt Express. 2017; 8:349–366. [Accessed May 21, 2018] Available at: https://www.ncbi.nlm.nih.gov/pmc/articles/PMC5231304/pdf/349.pdf. [PubMed: 28101423]

Author Manuscript

Author Manuscript

Author Manuscript

Author Manuscript

60. Manapuram RK, Manne VGR, Larin KV. Development of phase-stabilized swept-source OCT for the ultrasensitive quantification of microbubbles. Laser Phys. 2008; 18:1080–1086. [Accessed May 21, 2018] Available at: http://bol.egr.uh.edu/sites/bol/files/files/publications/Development-of-phase-stabilized-swept-source-OCT.pdf.

61. Wang S, Larin KV. Shear wave imaging optical coherence tomography (SWI-OCT) for ocular tissue biomechanics. Opt Lett. 2014; 39:41–44. [Accessed May 21, 2018] Available at: https://www.ncbi.nlm.nih.gov/pmc/articles/PMC4057602/pdf/nihms-596289.pdf. [PubMed: 24365817]

62. Song S, Huang Z, Wang RK. Tracking mechanical wave propagation within tissue using phase-sensitive optical coherence tomography: motion artifact and its compensation. J Biomed Opt. 2013; 18:121505. [PubMed: 24150274]

63. Mandell RB. Corneal power correction factor for photorefractive keratectomy. J Refract Corneal Surg. 1994; 10:125–128. [PubMed: 7517285]

64. Nguyen T-M, Song S, Arnal B, Wong EY, Huang Z, Wang RK, O'Donnell M. Shear wave pulse compression for dynamic elastography using phase-sensitive optical coherence tomography. J Biomed Opt. 2014; 19:016013. [Accessed May 21, 2018] Available at: https://www.ncbi.nlm.nih.gov/pmc/articles/PMC3894424/pdf/JBO-019-016013.pdf.

65. Kampmeier J, Radt B, Birngruber R, Brinkmann R. Thermal and biomechanical parameters of porcine cornea. Cornea. 2000; 19:355–363. [PubMed: 10832699]

66. Singh M, Han Z, Nair A, Schill A, Twa MD, Larin KV. Applanation optical coherence elastography: noncontact measurement of intraocular pressure, corneal biomechanical properties, and corneal geometry with a single instrument [letter]. J Biomed Opt. 2017; 22:20502. [Accessed May 21, 2018] Available at: https://www.ncbi.nlm.nih.gov/pmc/articles/PMC5316890/pdf/JB. [PubMed: 28241272]

67. Chan T, Payor S, Holden BA. Corneal thickness profiles in rabbits using an ultrasonic pachometer. Invest Ophthalmol Vis Sci. 1983; 24:1408–1410. [Accessed May 21, 2018] Available at: http://iovs.arvojournals.org/article.aspx?articleid=2159405. [PubMed: 6618800]

68. Cherfan D, Verter EE, Melki S, Gisel TE, Doyle FJ Jr, Scarcelli G, Yun SH, Redmond RW, Kochevar IE. Collagen cross-linking using rose bengal and green light to increase corneal stiffness. Invest Ophthalmol Vis Sci. 2013; 54:3426–3433. [Accessed May 21, 2018] Available at: http://iovs.arvojournals.org/article.aspx?articleid=2189439. [PubMed: 23599326]

69. Hatami-Marbini H, Rahimi A. Interrelation of hydration, collagen cross-linking treatment, and biomechanical properties of the cornea. Curr Eye Res. 2016; 41:616–622. [PubMed: 26126201]

70. Evans A, Whelehan P, Thomson K, McLean D, Brauer K, Purdie C, Baker L, Jordan L, Rauchhaus P, Thompson A. Invasive breast cancer: relationship between shear-wave elastographic findings and histologic prognostic factors. Radiology. 2012; 263:673–677. [Accessed May 21, 2018] Available at: https://pubs.rsna.org/doi/pdf/10.1148/radiol.12111317. [PubMed: 22523322]

71. Chang JM, Moon WK, Cho N, Yi A, Koo HR, Han W, Noh D-Y, Moon H-G, Kim SJ. Clinical application of shear wave elastography (SWE) in the diagnosis of benign and malignant breast diseases. Breast Cancer Res Treat. 2011; 129:89–97. [PubMed: 21681447]

72. Cross SE, Jin Y-S, Rao J, Gimzewski JK. Nanomechanical analysis of cells from cancer patients. Nat Nanotechnol. 2007; 2:780–783. [PubMed: 18654431]

73. Li QS, Lee GYH, Ong CN, Lim CT. AFM indentation study of breast cancer cells. Biochem Biophys Res Commun. 2008; 374:609–613. [PubMed: 18656442]

74. Han Z, Aglyamov SR, Li J, Singh M, Wang S, Vantipalli S, Wu C, Liu C-h, Twa MD, Larin KV. Quantitative assessment of corneal viscoelasticity using optical coherence elastography and a modified Rayleigh–Lamb equation. J Biomed Opt. 2015; 20(2):020501. [Accessed May 21, 2018] Available at: https://www.ncbi.nlm.nih.gov/pmc/articles/PMC4315865/pdf/JBO-020-020501.pdf.

75. Singh M, Li J, Han Z, Vantipalli S, Liu C-H, Wu C, Raghunathan R, Aglyamov SR, Twa MD, Larin KV. Evaluating the effects of giboflavin/UV-A and rose-bengal/green light cross-linking of the rabbit cornea by noncontact optical coherence elastography. Invest Ophthalmol Vis Sci. 2016; 57:OCT112–OCT120. [Accessed May 21, 2018] Available at: https://www.ncbi.nlm.nih.gov/pmc/articles/PMC4968774/pdf/i1552-5783-57-9-OCT112.pdf. [PubMed: 27409461]

76. Kirby MA, Pelivanov I, Song S, Ambrozinski Ł, Yoon SJ, Gao L, Li D, Shen TT, Wang RK, O'Donnell M. Optical coherence elastography in ophthalmology. J Biomed Opt. 2017; 22:1–28.

[Accessed May 21, 2018] Available at: https://pdfs.semanticscholar.org/de93/fcf0c44e45f989bcd136f789c4d9076d793f.pdf?_ga=2.145844663.28271886.1526907271-1896146218.1520269055.

77. Thomasy SM, Raghunathan VK, Winkler M, Reilly CM, Sadeli AR, Russell P, Jester JV, Murphy CJ. Elastic modulus and collagen organization of the rabbit cornea: epithelium to endothelium. Acta Biomater. 2014; 10:785–791. [Accessed May 21, 2018] Available at: https://www.ncbi.nlm.nih.gov/pmc/articles/PMC4280096/pdf/nihms531916.pdf. [PubMed: 24084333]

78. Wollensak G, Iomdina E. Long-term biomechanical properties of rabbit cornea after photodynamic collagen crosslinking. Acta Ophthalmol. 2009; 87:48–51. [Accessed May 21, 2018] Available at: http://onlinelibrary.wiley.com/doi/10.1111/j.1755-3768.2008.01190.x/pdf. [PubMed: 18547280]

79. Bueno JM, Gualda EJ, Giakoumaki A, Pérez-Merino P, Marcos S, Artal P. Multiphoton microscopy of ex vivo corneas after collagen cross-linking. Invest Ophthalmol Vis Sci. 2011; 52:5325–5331. [Accessed May 21, 2018] Available at: http://iovs.arvojournals.org/article.aspx?articleid=2187615. [PubMed: 21467175]

80. Elsheikh A, Wang D, Brown M, Rama P, Campanelli M, Pye D. Assessment of corneal biomechanical properties and their variation with age. Curr Eye Res. 2007; 32:11–19. [PubMed: 17364730]

81. Hedbys BO, Mishima S. The thickness–hydration relationship of the cornea. Exp Eye Res. 1966; 5:221–228. [PubMed: 5914654]

82. Han Z, Li J, Singh M, Wu C, Liu C-h, Wang S, Idugboe R, Raghunathan R, Sudheendran N, Aglyamov SR, Twa MD, Larin KV. Quantitative methods for reconstructing tissue biomechanical properties in optical coherence elastography: a comparison study. Phys Med Biol. 2015; 60:3531–3547. [Accessed May 21, 2018] Available at: https://www.ncbi.nlm.nih.gov/pmc/articles/PMC4409577/pdf/nihms681019.pdf. [PubMed: 25860076]

83. Doyle JF. Wave Propagation in Structures; Spectral Analysis Using Fast Discrete Fourier Transform. 2. New York, NY: Springer; 1997. 198–242.

84. Wang S, Larin KV. Noncontact depth-resolved micro-scale optical coherence elastography of the cornea. Biomed Opt Express. 2014; 5:3807–3821. [Accessed May 21, 2018] Available at: https://www.ncbi.nlm.nih.gov/pmc/articles/PMC4242019/pdf/3807.pdf. [PubMed: 25426312]

85. Tanter M, Touboul D, Gennisson J-L, Bercoff J, Fink M. High resolution quantitative imaging of cornea elasticity using supersonic shear imaging. IEEE Trans Med Imaging. 2009; 28:1881–1893. [PubMed: 19423431]

86. Zhang X, Yin Y, Guo Y, Fan N, Lin H, Liu F, Diao X, Dong C, Chen X, Wang T, Chen S. Measurement of quantitative viscoelasticity of bovine corneas based on Lamb wave dispersion properties. Ultrasound Med Biol. 2015; 41:1461–1472. [Accessed May 21, 2018] Available at: http://or.nsfc.gov.cn/bitstream/00001903-5/345244/1/1000013947733.pdf. [PubMed: 25638310]

87. Singh M, Wu C, Liu C-H, Li J, Schill A, Nair A, Larin KV. Phase-sensitive optical coherence elastography at 1. 5 million A-Lines per second. Opt Lett. 2015; 40:2588–2591. [Accessed May 21, 2018] Available at: https://www.ncbi.nlm.nih.gov/pmc/articles/PMC5451255/pdf/nihms859350.pdf. [PubMed: 26030564]

WHAT WAS KNOWN

- Corneal hydration alters the geometry and biomechanical properties of the cornea.

WHAT THIS PAPER ADDS

- Young's modulus of the cornea increased as the cornea thinned as a result of dehydration.

Results show that Young's modulus of the cornea is a factor of the thickness and hydration states that should be taken into account for proper quantification of the cornea's biomechanical properties.
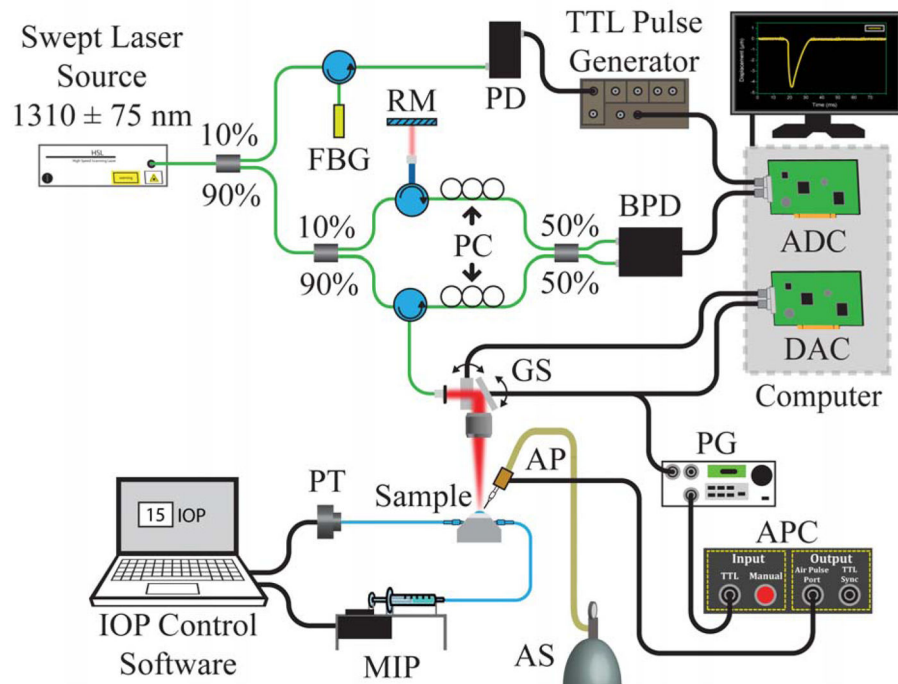
Figure 1.
Schematic of the experimental setup (ADC = analog-to-digital converter; AP = air-pulse port; APC = air-pulse controller; AS = air supply; BPD = balanced photodetector; DAC = digital-to-analog converter; FBG = fiber-Bragg grating; GS = galvanometer-mounted mirror scanners; IOP = intraocular pressure; MIP = microinfusion pump; PC = polarization controller; PD = photodetector; PG = pulse generator; PT = pressure transducer; RM = reference mirror; TTL = transistor–transistor logic).
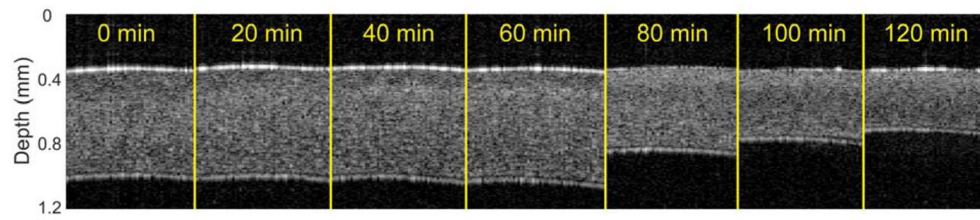
Figure 2.
Optical coherence tomography structural images of the central region of approximately 2.0 mm a typical cornea after rescaling to physical dimensions. Topical PBS was dropped for the first 60 minutes, after which a 20% dextran solution was dropped on the corneas for an additional 60 minutes (PBS = phosphate-buffered saline).
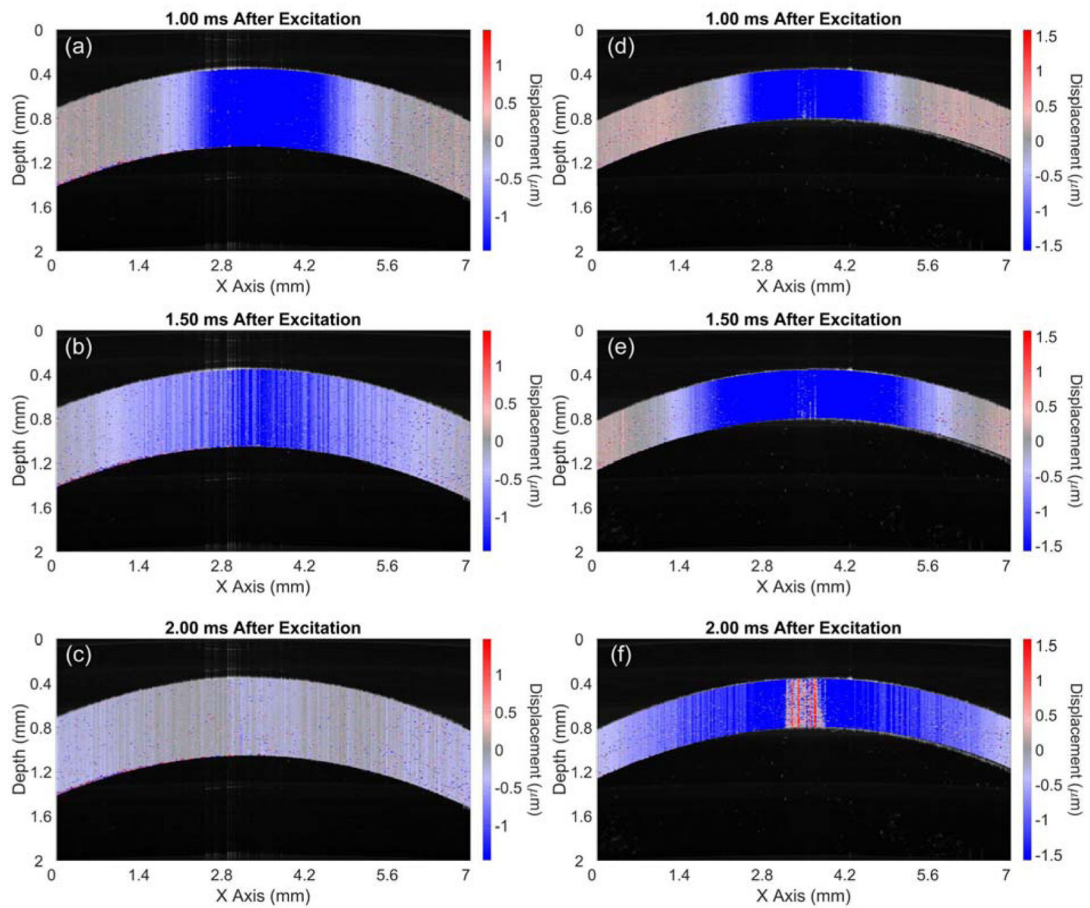
Figure 3.
Air pulse–induced elastic-wave propagation in a typical sample at the initial 0-minute measurement (*a* to *c*) and the 100-minute measurement (*d* to *f*) (see Video 1, available at: http://jcrsjournal.org). The time after the air-pulse excitation for each frame is shown above the corresponding image.
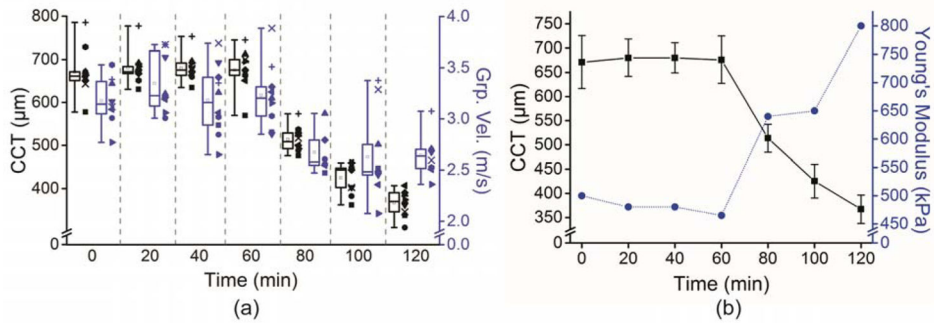
Figure 4.

a: The CCT and elastic-wave group velocity of all 10 samples plotted as a function of time. The CCT is represented in black, and the elastic-wave group velocity is represented in blue. Each sample is coded by the shape of the datapoints plotted alongside the corresponding box-and-whisker plot. The boxes are the interquartile range, the central line is the median, the whiskers are the 5th and 95th percentiles, and the small inscribed box is the mean. *b*: Averaged CCT and Young's modulus quantified by the finite element method. The CCT is represented by the black squares and solid black line, and the Young's modulus is represented by the blue circles and dotted blue line. The error bars are the intersample SD. A 0.9% PBS solution was dropped on the corneas for the first 60 minutes, and a 20% dextran solution was dropped on the corneas for an additional 60 minutes (CCT = central corneal thickness; Grp. Vel. = group velocity; PBS = phosphate-buffered saline).